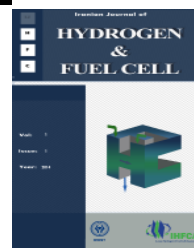


Iranian Journal of Hydrogen & Fuel Cell

IJHFC

Journal homepage://ijhfc.irost.ir



## Physical properties and electronic structure of $\text{LaNi}_5$ compound before and after hydrogenation: An experimental and theoretical approach

Seyyed Mojtaba Zareii (Alavi Sadr)<sup>1</sup>, Hadi Arabi<sup>1,2,\*</sup>, Faiz Pourarian<sup>3</sup>, Reza Sarhaddi<sup>1</sup>

<sup>1</sup> Magnetism and Superconducting Research Laboratory, Department of Physics, Faculty of Science, University of Birjand, Birjand, Iran.

<sup>2</sup> Department of Physics, Faculty of Science, Ferdowsi University of Mashhad, Mashhad, Iran.

<sup>3</sup> Department of Material Science and Engineering, Carnegie Mellon University, Pittsburgh, PA, USA.

### Article Information

Article History:

Received:

4 August 2013

Received in revised form:

5 October 2013

Accepted:

14 January 2014

### Keywords

Hydrogen storage

$\text{LaNi}_5$

Hydriding kinetic

Density functional theory

Heat of formation

### Abstract

The present study deals with the experimental and theoretical approaches of  $\text{LaNi}_5$  hydrogen storage alloy. The structural, morphological and hydrogenation characterization of this sample which is synthesized by the arc melting technique were carried out by X-ray diffraction, scanning electron microscopy and a homemade Sievert's type apparatus, respectively. The results showed that after several hydrogenation/dehydrogenation cycles, disproportionation occurs in  $\text{LaNi}_5$ . The hydriding kinetic measurements under different applied pressures show that the hydrogen storage capacity (Cwt.%) increases with pressure. However, kinetic analysis at different temperatures under constant initial pressure, which is fitted to two models such as Jander diffusion model and Johnson-Mehl-Avrami, revealed that Cwt.% and hydriding reaction rate are decreased and increased by increasing temperature, respectively.

The theoretical study using full potential linearized augmented plane wave plus local orbitals method was also performed to investigate the structural, energetic and electronic properties of  $\text{LaNi}_5$  and its saturated hydride ( $\text{LaNi}_5\text{H}_7$ ). From the two possible space groups for  $\text{LaNi}_5\text{H}_7$ ,  $P6_3mc$  was found as the most favorable one. A volume expansion of  $\sim 26\%$  was found for its hydride. Other calculated results including the equilibrium atomic positions, bulk modulus and the enthalpy of formation were in good agreement with other theoretical and experimental results. The band structure calculations showed that the valence bands were mainly derived from Ni-3d states, and the bandwidth of the occupied Ni-3d bands in hydride phase was narrower than that of the parent compound due to the filling of Ni-3d bands as a result of hydrogen absorption and volume expansion.

\*Corresponding author. E-mail: arabi\_h@birjand.ac.ir & arabi-h@um.ac.ir  
Tel: 0511-8796416, Fax: 0511-8796983

## 1. Introduction

The limited fossil fuel resources and the environmental impact of their use require a change to renewable energy sources (wind, solar, biomass, geothermal, hydropower, hydrogen and fuel cell) in the near future [1]. For mobile application, an efficient energy carrier is needed that can be produced and used in a closed cycle. Presently, hydrogen is the only energy carrier that can be produced easily in large quantities and in an appropriate time scale. However, the absence of a practical means for hydrogen storage has brought about a major difficulty in utilizing hydrogen as a fuel or energy carrier [2]. A solid hydrogen storage system, like metal hydrides, is reliable, simple to fabricate and much safer than the use of other phases of hydrogen. The metal hydrides still attract highest attention because of their applications in a wide range of industrial fields such as hydrogen storage media for fuel cells and internal combustion engines, electrodes for rechargeable batteries, and energy conversion materials [3]. In particular, LaNi<sub>5</sub> alloy is of great technological interest in its applications, such as compressors, heat pumps, rechargeable batteries and energy conversion materials [3-5]. Furthermore, LaNi<sub>5</sub>-H system is accepted as a prototype of hydrogen absorbing materials for its excellent hydrogenation properties. The hydrogen storage capacity for LaNi<sub>5</sub> is about 1.38 wt.% which exceeds that of liquid hydrogen [6].

On the theoretical side, the band structure and chemical nature of the parent compound play key roles in the performance and hydriding properties as they determine the hydrogen storage capacity (Cwt.%), intrinsic kinetics, as well as the operating temperature and pressure range [7]. For example, in LaNi<sub>5</sub>-based compounds, it is well known that the state of vacancy of the Ni-3d level controls the hydrogen storage capacity as the 4s and 3d band overlap [8]. Besides, from the stability perspective, the measured heat of formation ( $\Delta H$ ) for LaNi<sub>5</sub> hydride at high hydrogen density is found experimentally to be about -32 kJ/mol.H<sub>2</sub> [9]. However, recent theoretical calculations could not predict the correct heat of formation for LaNi<sub>5</sub> hydrides. Tatsumi et al. [10] studied the heat of formation of LaNi<sub>5</sub>H<sub>7</sub> by a plane-wave basis pseudo-potential method and obtained -45 kJ/mol.H<sub>2</sub>, which is approximately 50% more negative than the experimental value. This has discouraged using first-principles total energy methods in the search for novel metal hydrides. Hector et al. [11] improved these results

by employing the well-known pseudo-potential plane-wave (PP-PW) method and obtained -40 kJ/mol.H<sub>2</sub> for  $\Delta H$ . It should also be noted that the saturated LaNi<sub>5</sub> hydride (LaNi<sub>5</sub>H<sub>7</sub>;  $\beta$  phase) is experimentally characterized in two different space groups (SGs), namely P6<sub>3</sub>mc and P31c phases [12-13]. Neither of the two possible SGs could be discarded by a neutron diffraction experimental characterization or pseudo-potential (PP) theoretical approach [11], while all-electron calculations using augmented spherical wave (ASW) claimed that SG P6<sub>3</sub>mc is more stable [13]. However, the SG P6<sub>3</sub>mc can be preferred primarily because its crystallography is somewhat simpler [11]. So, it can be instructive to investigate the stability of  $\beta$  phase hydride systems by the full-potential linearized augmented plane wave plus local orbitals (FP-LAPW+lo), which is the most accurate one for band structure calculations [14]. In this paper, the synthesis details and physical properties of pure LaNi<sub>5</sub> and its hydride based on their structural and absorption kinetic characterization were investigated. Moreover, the theoretical study of structural, energetic and electronic properties of this compound and its  $\beta$  hydride were followed using FP-LAPW+lo method implemented in Wien2k code [15].

## 2. Experimental and theoretical details

### 2.1. Experimental details: synthesis and characterization details

The LaNi<sub>5</sub> alloy was prepared in an arc furnace under high purity argon atmosphere (99.999%) with stoichiometric proportion of constituent elements. The obtained alloy ingot was turned over and re-melted three times for obtaining more homogeneity. Then, the ingot was mechanically crushed and ground into the powder of 200 mesh size for X-ray diffraction (XRD) characterization and kinetics curves. The crystal structure and lattice parameters of the alloy before and after hydrogenation/dehydrogenation cycles were determined by XRD (X'Pert Pro, PANalytical system) with Cu-K $\alpha$  radiation ( $\lambda = 1.5406 \text{ \AA}$ ). The plasma-optical emission spectroscopy (model: Varian Vista Pro ICP-OES) was used to investigate the composition of alloy. To study the kinetics behavior of LaNi<sub>5</sub> alloy, first a homemade Sievert's type apparatus was designed and fabricated in our laboratory as shown in Fig. 1. This apparatus works according to the pressure reduction in determined volumes [2].

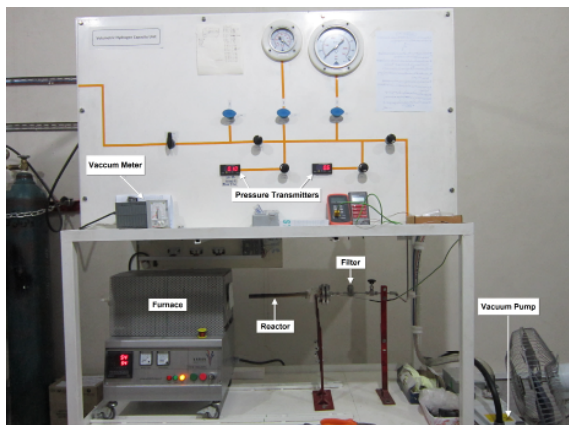


**Figure 1. A schematic of the homemade Sievert's type apparatus which is used in our studies.**

For hydrogenation measurements, about 2g of powder sample was introduced into the reactor. Then the reactor was evacuated to  $\sim 10^{-3}$  Torr at room temperature and heated up to 673 K for 2h in vacuum. The high purity hydrogen (99.999%) with 6 MPa pressure was applied to the reactor for 60 min after which the sample cooled down to room temperature. By repeating this process several times, the sample became completely activated and ready for measurement of absorption kinetic plots.

## 2.2. Computational details: crystal structures and computational methodology

$\text{LaNi}_5$  crystallizes in the hexagonal  $\text{CaCu}_5$ -type structure (SG  $\text{P6}/\text{mmm}$ ) as La atoms occupy 1a sites and Ni atoms occupy 2c and 3g sites. Hydrogenation of  $\text{LaNi}_5$ , up to maximum hydrogen uptake brings modifications of the crystal structure with two possible space groups for  $\text{LaNi}_5\text{H}_7$  ( $\beta$  phase), i.e.  $\text{P6}_3\text{mc}$  and  $\text{P31c}$ , determined by neutron diffraction data [13]. These show a supercell unit ( $2 \times \text{LaNi}_5\text{H}_7$ ), i.e.  $\text{La}_2\text{Ni}_{10}\text{H}_{14}$ , along the c-axis [13]. The only difference between the two structures is a mirror plane that leads to (x, x-, z) coordinates for 6c sites in  $\text{P6}_3\text{mc}$  instead of (x, y, z) in  $\text{P31c}$  [13, 11]. There are one La (2a), three Ni (2b, 2b and 6c) and three H (2b, 6c and 6c) sites in  $\beta$ -hydride structure of  $\text{LaNi}_5$  [13].

In this work, the theoretical calculations of structural, energetic and electronic properties of  $\text{LaNi}_5$  compound and its saturated hydride ( $\text{LaNi}_5\text{H}_7$ ) were performed using FP-LAPW+lo method as implemented in the WIEN2k code [15]. The generalized gradient approximation (GGA) of PBE96 [16] was used as exchange correlation functional. The muffin-tin sphere radii  $R_{\text{mt}}$  are chosen as 2.35, 2.21 and 0.9 bohr for La, Ni and

H atoms, respectively. The size of the basis set is given by the product  $R_{\text{mt}} \times K_{\text{max}} = 7.0$  ( $\text{LaNi}_5$ ) and 5.0 ( $\text{LaNi}_5\text{H}_7$ ), where  $K_{\text{max}}$  is the largest reciprocal space wave vector in the basis set. A cutoff energy of -6.0 Ry was chosen between valence and core states. The maximum value of  $l$  was taken as  $l_{\text{max}} = 10.0$ , and the charge density is Fourier expanded up to  $G_{\text{max}} = 14.0$  ( $\text{LaNi}_5$ ) and 18.0 ( $\text{LaNi}_5\text{H}_7$ ). A mesh of 133 ( $\text{LaNi}_5$ ), 76 ( $\text{LaNi}_5\text{H}_7$  in  $\text{P6}_3\text{mc}$ ) and 100 ( $\text{LaNi}_5\text{H}_7$  in  $\text{P31c}$ ) k-points in the irreducible Brillouin zone (IBZ) was used for BZ integration with a modified tetrahedron method [17] to guarantee the convergence of total energy. Self-consistency was achieved by demanding the charge convergence criterions set to  $10^{-5}$  Ry and  $10^{-4}$  electrons, simultaneously. In the following, the saturated hydride phases crystallizing with SGs  $\text{P6}_3\text{mc}$  and  $\text{P31c}$  will be referred to as  $\beta_1$  and  $\beta_2$ , respectively.

## 3. Results and discussion

### 3.1. Experimental work

#### 3.1.1. X-ray and microstructure characterizations

Figures 2a-2c show the XRD patterns of as-synthesized, hydrogenated and dehydrogenated  $\text{LaNi}_5$  alloys (after 30 cycles), respectively. The results of structural parameters including the lattice parameters, unit cell volumes, overall broadening at full width at half maximum (FWHM) of the main peak (111), crystallites size and lattice strain of  $\text{LaNi}_5$  alloy are listed in Table 1.

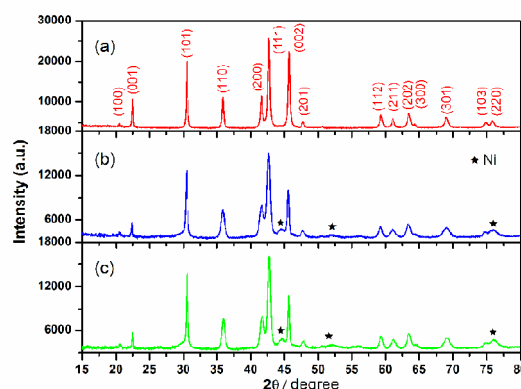


**Figure 2. XRD patterns of (a) as-synthesized, (b) hydrogenated and (c) dehydrogenated  $\text{LaNi}_5$  alloy.**

The XRD pattern of as-synthesized LaNi<sub>5</sub> alloy (Fig. 2a) indicates that parent bulk alloy is homogeneous with a single phase corresponding to CaCu<sub>5</sub>-type hexagonal structure (SG: P6/mmm; JCPDS/PDF No.: 50-0777). However, for hydrogenated and dehydrogenated LaNi<sub>5</sub> alloy after hydrogenation/dehydrogenation through several cycles, in addition to CaCu<sub>5</sub>-type hexagonal structure as a main phase, a small amount of free Ni (SG: Fm-3m; JCPDS/PDF no.: 04-0850) also was detected (Figs. 2b & 2c). Appearance of Ni phase that has been also reported in the literature [18-19] is due to disproportionation process [2] that can be disappeared by different methods such as heat treatment of the as-casted LaNi<sub>5</sub> alloy [20]. On the other hand, intensity of peaks (especially for most intense peak) is decreased for hydrogenated/dehydrogenated samples that indicated decreasing of crystallinity of alloy after several hydrogenation/dehydrogenation (H/D) cycles. Also, H/D process caused overall (observed) broadening of the XRD peaks. For quantitative description of this result, the crystallite sizes and the microstrains could be calculated from the broadening diffraction peaks [21].

The overall broadening of the diffraction peak (observed) contains the instrumental and physical broadening. The physical broadening ( $\beta^p$ ) is comprised of two effects: one arising from the average crystallite size ( $D$ ) and the other from the microstrain ( $\epsilon$ ) [21]. In order to obtain  $\beta^p$ , the instrumental broadening should be eliminated from the overall broadening of samples. We used the pure Si sample for calculation of instrumental broadening. The broadening effects caused by crystallite size and microstrain were separated by using Williamson-Hall and least square fit method [21]:

$$\frac{\beta^p \cos \theta}{\lambda} = \frac{0.89}{D} + \epsilon \frac{4 \sin \theta}{\lambda} \quad (1)$$

From the slope and the ordinate intercept of Williamson-Hall plot, i.e.  $\beta^p \cos \theta / \lambda$  versus  $4 \sin \theta / \lambda$ , the microstrain and the crystallite size were determined and presented in Table 1.

**Table 1. Structural parameters, FWHM (111), crystallite size and microstrain of different samples.**

Sample	Phases	Lattice parameters		Unit cell volume	FWHM (111) [°]	D [nm]	$\epsilon$ [%]
		a [Å]	c [Å]	V [Å <sup>3</sup> ]			
As-synthesized	LaNi <sub>5</sub>	5.0182	3.9816	86.833	0.3034	157	0.094
	LaNi <sub>5</sub> H <sub>0.3</sub>	5.0241	4.0085	87.6252	0.5210	104	0.28
Hydrogenated	Ni	3.5447	-	44.5388	-		
	Dehydrogenated	LaNi <sub>5</sub>	5.0153	3.9956	87.0380	0.4417	137
Ni		3.5315	-	44.043	-		

By comparing the results, it can be concluded that the lattice strains are introduced by the cycling process [1], and a decrease in particle size was found due to the lattice expansion on hydrogenation [18]. The calculated crystallite size of the as-synthesized sample was 157 nm which reduced to 104 nm after hydrogenation (30 cycles) and 137 nm after dehydrogenation due to the lattice strain caused by the defects generated from hydrogen cycling [21].

Comparison of structural parameters of hydrogenated LaNi<sub>5</sub> alloy with as-synthesized indicates an increase in lattice parameters and unit cell volume due to hydrogen insertion in interstitial positions. It must be noted that plateau pressure of LaNi<sub>5</sub>-H system at room temperature is higher than atmospheric pressure, so once the hydrogenated LaNi<sub>5</sub> alloy (full hydride) was put in ambient conditions, most of the hydrogen absorbed by the alloy was desorbed from hydride. Nonetheless, a very small percentage of absorbed hydrogen still remains that detected by XRD results as LaNi<sub>5</sub>H<sub>x</sub> ( $x \sim 0.3$ ). Beside, a countable increase is found in the lattice parameter 'c' in dehydrogenated alloy in comparison to as-synthesized alloy, whereas a very small decrease is observed in the lattice parameter 'a'. These decrease and increase observed in the lattice parameters are probably due to presence of strain and residual hydrogen in the lattice of the alloy after hydrogenation/dehydrogenation cycles, respectively [22-23].

To investigate the effect of H/D cycling on the surface morphology and microstructure of LaNi<sub>5</sub> alloy powder, the SEM images of back-scattered electrons of particles were taken at different magnifications both before (Figs. 3a, b) and after 30 H/D cycles (Figs. 3c, d). It is well observed that after H/D cycling, the particle size decreases, mostly lower than 10-20 nm, and they have nearly uniform size distribution compared to non-cycled ingots. The internal stress created in lattice due to the volume expansion (shrinkage) from hydrogen absorption (desorption) is really the driving force to lead to the pulverization of the alloy [24, 25]. On the other hand, no crack was found in the non-cycled alloy, while some cracks were developed on the surface of the alloys after H/D cycles. Formation of new small grains might be resulting from propagations of these microcracks [25].

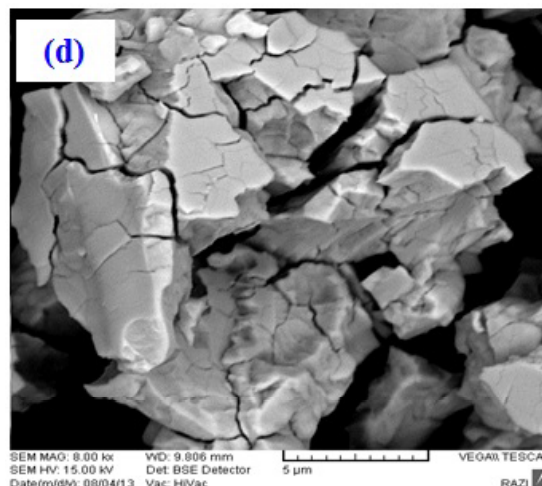
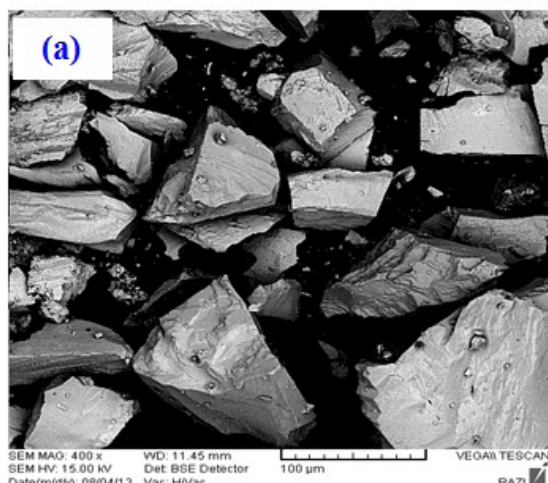
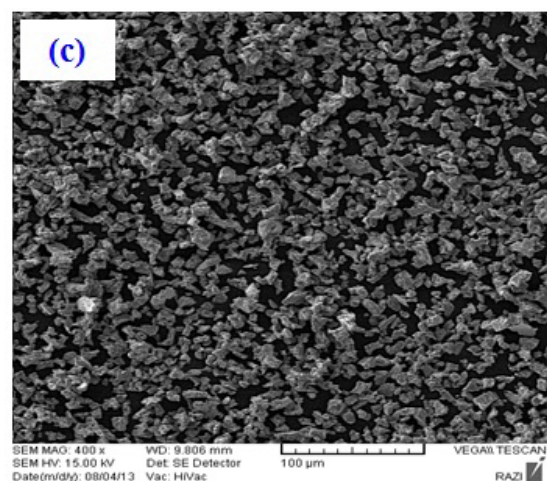
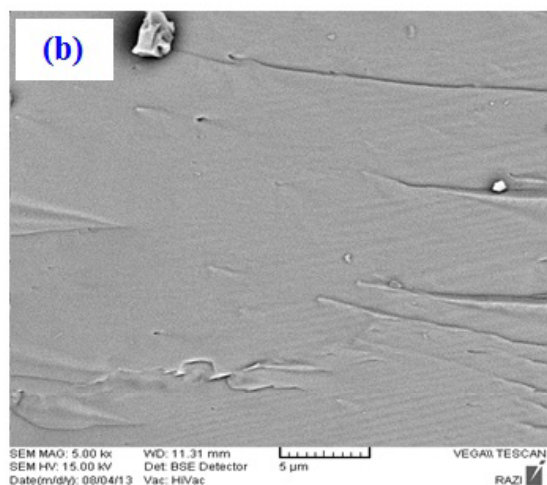


Figure 3. SEM images of (a and b) alloy ingots put in the reactor before hydrogenation; (c and d) the alloy after 30 H/D cycles.



### 3.1.2. Hydrogen absorption kinetics

The hydriding kinetic measurements of  $\text{LaNi}_5$  alloy, after 30 hydriding/dehydriding cycles, were carried out within two schemes: (i) absorption kinetic at constant temperature under different applied pressures, and (ii) absorption kinetic at different temperatures ( $T=20, 40$  and  $60^\circ\text{C}$ ) under constant initial pressure for  $\text{H}_2$  (4 MPa). The hydrogen absorption kinetic plots of  $\text{LaNi}_5$  at  $40^\circ\text{C}$  for different hydrogen pressures are shown in Fig. 4. The hydrogen storage capacity (Cwt.%) is defined as the ratio between the mass of the absorbed hydrogen and mass of the hydride. As can be seen, the hydrogen storage capacity of  $\text{LaNi}_5$  significantly increases with an increment in hydrogen applied pressure: 0.53, 0.97, 1.12, 1.21, 1.32% for 0.5, 1, 2, 3, 4 MPa hydrogen pressures, respectively. The increase in the hydrogen storage capacity as a function of applied pressure can be explained as follows: with increase in initial pressure, the hydrogen gas concentration on the surface of  $\text{LaNi}_5$  particles is increased which results in the increase of the effective pressure or the pressure driving force in excess of the equilibrium pressure [26].

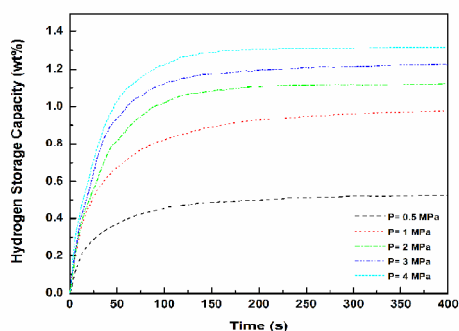


Figure 4. The hydriding kinetic plots of the  $\text{LaNi}_5$  at  $40^\circ\text{C}$  under different pressures.

Hence, both the absorption kinetic and hydrogen storage capacity (Cwt.%) increase. It should be noted that since working temperature is constant for all initial pressures, therefore, its catalytic effect for the dissociation of the  $\text{H}_2$  molecules to H atoms has the same contribution for different pressures.

Fig. 5 shows the influence of operating temperatures on the hydrogen absorption kinetics of  $\text{LaNi}_5$  hydride alloy under a constant initial pressure of  $\text{H}_2$  (4MPa). It can be seen that hydriding reaction rates increase with operating temperature. However, it is found that hydrogen storage capacity (Cwt.%) decreases with increasing temperature. The observed increase and decrease for absorption reaction rate and hydrogen capacity can be understood from the catalytic effect of temperature and from the reversible hydrogen absorption/desorption on the surface of  $\text{LaNi}_5$  grain, respectively. With increase in temperature, more and more hydrogen is desorbed during the

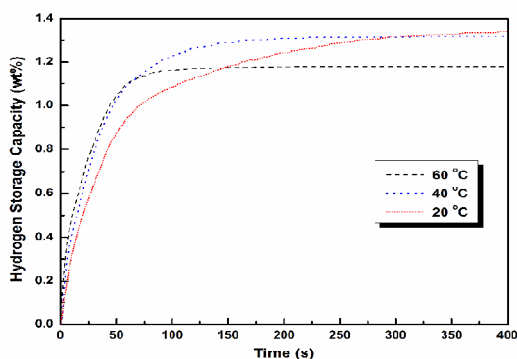


Figure 5. The hydriding kinetics plots of the  $\text{LaNi}_5$  at different temperatures.

hydrogen absorption processes, resulting in the decrease of the hydrogen capacity for  $\text{LaNi}_5$  alloy [27]. As the working temperature increases, more  $\text{H}_2$  molecules are dissociated to H atoms [28]. That is why that reaction rate increases with temperature.

The mechanism of hydriding reaction kinetics was studied by using different fitting models. In the literature, different models [29-35] have been proposed. The most extended model is the Johnson-Mehl-Avrami model [35] which has been validated with different sorption experimental data, not only for  $\text{LaNi}_5$ , but also for other alloys [31]. In this work, Jander diffusion model (JDM) [34], first order and antilog Johnson-Mehl-Avrami (JMA) models [35] were employed as fitting models to analyze the hydriding reaction mechanisms of  $\text{LaNi}_5$  (Table 2).

Table 2. Some conventional fitting models used for hydriding reaction kinetic.

Kinetic model	Comments
$\xi = 1 - (1 - \sqrt{kt})^3$	Jander diffusion model (JDM)
$\xi = 1 - \exp[-kt]$	Johnson-Mehl-Avrami (JMA) model: first order
$\xi = 1 - \exp[-kt^n]$	Johnson-Mehl-Avrami (JMA): antilog model

In these models,  $\xi(t)$ ,  $k$  and  $n$  are the reacted fraction at any time ( $t$ ), and the rate constant and order of reaction, respectively. The  $\xi(t)$  is defined as the ratio between the mass of sample at time  $t$  and that of saturated sample at infinite time. In JDM model, the particles are considered as spherical in shape, and diffusion is the only rate-controlling mechanism [34], whereas JMA model includes both diffusion and nucleation and growth as the rate-controlling mechanisms [35]. It should be noted that the rate constant ( $k$ ) depends on temperature and supply pressure. For a constant temperature, plots of  $[1 - (1 - \xi)^{1/3}]^2$  and vs. time ( $t$ ), respectively for JDM and first order JMA models, are the straight lines with slope  $k$ , whereas for antilog JMA model, a plot of vs. is a straight line with slope  $n$  and intersect  $\ln(k)$ . The rate constants obtained at different temperatures using different models altogether,  $R^2$ , as the linear regression are presented in Table 3.

It can be seen that the hydriding reaction rate increases with increasing the temperature within all models. For JDM model, the derivation of experimental data is rather larger for the high temperature ( $60^\circ\text{C}$ ) as previously reported by Muthukumar et al. [30]. The  $R^2$  of the linear regression equations of the JMA antilog model is slightly more than those of JMA first order and

also JDM model for 20 and 40°C, while  $R^2$  of the JMA first order model is the highest at the high

good agreement with those of [30].

**Table 3. Calculated rate constants for different temperatures using JDM and JMA models.**

Kinetic model	Temperature, (°C)	rate constant $k$ , (ms) <sup>-1</sup>	$R^2$ , (%)
JDM model	20	1.73	99.87
	40	3.43	99.76
	60	5.66	98.54
First order JMA	20	13.88	98.39
	40	26.11	99.74
	60	44.47	99.88
Antilog model JMA	20	36.2	99.9
	40	55.35	99.82
	60	96.68	99.07

temperature (60 °C).

Therefore, the JMA model is superior to the JDM model in analyzing the absorption reaction kinetic mechanism of  $\text{LaNi}_5$ , and hence diffusion along with nucleation and growth is the rate-controlling step.

Using the values of constant rate evaluated from different models, the activation energy  $E_a$  of hydriding reaction was calculated by Arrhenius relationship:

$$k = Ae^{\left(\frac{-E_a}{RT}\right)} \quad (2)$$

where  $A$  and  $R$  is the pre-exponential factor and universal gas constant, respectively. A plot of  $\ln(k)$  vs.  $1/T$  is a straight line with slope  $E_a/R$  as shown in Fig. 6 for JDM and JMA models.

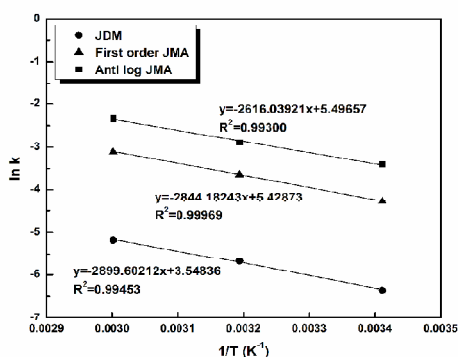


**Figure 6. Arrhenius plot for  $\text{LaNi}_5$  with different models.**

The estimated values of  $E_a$  are 24.11, 23.65 and 21.75 kJ/mol. $\text{H}_2$  for JDM, first order and antilog JMA models respectively. These results are in

## 3.2. Theoretical work

### 3.2.1. Equilibrium structural properties

In the first step, a geometry optimization was carried out on  $\text{LaNi}_5$  (parent alloy) and  $\text{LaNi}_5\text{H}_7$  (saturated hydride) using the FP-LAPW+lo scheme. To find which  $\beta$  phase models ( $\beta_1$  or  $\beta_2$ ) are the most stable, both space groups (SGs) were considered from a structural and energetic points of view. The starting internal parameters as well as the lattice constants were taken from the experiment [13]. The optimization results for lattice constants and equilibrium atomic Wyckoff positions obtained from the Murnaghan fit [36] and from minimizing the Hellmann-Feynman forces [37] are presented in Table 4. The other experimental and theoretical results are also listed for comparison. Our results show that the SG  $P6_3mc$  is more stable than the SG  $P31c$  (Fig. 7).

**Table 4. The calculated lattice parameters  $a$ ,  $c$  (Å), relaxed atomic positions and bulk modulus  $B_0$  (GPa). The corresponding experimental and theoretical values are also given for comparison.**

	This work		Other works	
	Theoretical	Experimental	Theoretical	Experimental
<b><math>\text{LaNi}_5</math> (<math>P6/mmm</math>)</b>				
$a$	5.008	5.0182	5.001 <sup>a</sup>	5.017 <sup>a</sup>
$c$	3.979	3.9816	3.963 <sup>a</sup>	3.986 <sup>a</sup>
$B_0$	138	-	134.9 <sup>a</sup> , 135 <sup>b</sup>	137 <sup>c</sup> , 139 <sup>d</sup> , 126.8 <sup>e</sup>
<b><math>\text{LaNi}_5\text{H}_7</math> (<math>P6_3mc</math>)</b>				
$a$	5.4094	-	5.332 <sup>a</sup>	5.409 <sup>a</sup>
$c$	8.6007	-	8.626 <sup>a</sup>	8.600 <sup>a</sup>
$B_0$	133	-	121 <sup>c</sup> , 122.9 <sup>a</sup>	-
La (2a)	(0, 0, 0.026)	-	(0, 0, 0.022) <sup>a</sup>	(0, 0, 0.022) <sup>a</sup>
Ni1 (6c)	(0.5005, -x, 0.249)	-	(0.499, -x, 0.252)	(0.498, -x, 0.250)
Ni2 (2b)	(1/3, 2/3, 0.003)	-	(1/3, 2/3, 0.006)	(1/3, 2/3, 0.002)
Ni3 (2b)	(1/3, 2/3, 0.482)	-	(1/3, 2/3, 0.482)	(1/3, 2/3, 0.489)
H1 (6c)	(0.505, -x, 0.056)	-	(0.504, -x, 0.056)	(0.506, -x, 0.059)
H2 (2b)	(1/3, 2/3, 0.816)	-	(1/3, 2/3, 0.814)	(1/3, 2/3, 0.819)
H3 (6c)	(0.157, -x, 0.280)	-	(0.148, -x, 0.275)	(0.160, -x, 0.280)
<b><math>\text{LaNi}_5\text{H}_7</math> (<math>P31c</math>)</b>				
$a$	5.4134	-	5.315 <sup>a</sup>	5.409 <sup>a</sup>
$c$	8.6070	-	8.492 <sup>a</sup>	8.600 <sup>a</sup>
$B_0$	132	-	122.7 <sup>a</sup> , 121 <sup>c</sup>	-
La (2a)	(0, 0, 0.034)	-	(0, 0, 0.025)	(0, 0, 0.004)
Ni1 (6c)	(0.501, 0.498, 0.252)	-	(0.500, 0.502, 0.258)	(0.517, -0.486, 0.250)
Ni2 (2b)	(1/3, 2/3, 0.008)	-	(1/3, 2/3, 0.011)	(1/3, 2/3, 0.006)
Ni3 (2b)	(1/3, 2/3, 0.483)	-	(1/3, 2/3, 0.488)	(1/3, 2/3, 0.497)
H1 (6c)	(0.507, 0.496, 0.058)	-	(0.506, 0.494, 0.066)	(0.510, -0.490, 0.037)
H2 (2b)	(1/3, 2/3, 0.821)	-	(1/3, 2/3, 0.825)	(1/3, 2/3, 0.83)
H3 (6c)	(0.160, 0.839, 0.291)	-	(0.146, 0.852, 0.278)	(0.154, -0.168, 0.299)

<sup>a</sup> Al Alam et al [13].

<sup>b</sup> Hector et al [11].

<sup>c</sup> Berezniatsky et al [39].

<sup>d</sup> Brouha et al [40].

<sup>e</sup> Tanaka et al [41].

The lattice constants and internal parameters calculated for the SG  $P6_3mc$  are also closer to those of the experimental values with respect to the SG  $P31c$ . The same trends were observed in other ab initio calculations [10, 13]. The calculated equilibrium volumes for  $\beta_1$  and  $\beta_2$  phases and for double unit cell of parent alloy ( $\text{La}_2\text{Ni}_{10} = 2 \times \text{LaNi}_5$ )

are 219.1, 219.8 and 172.8 Å<sup>3</sup>, respectively. The agreement between our theoretical results and experimental parameters is excellent in comparison with other reported theoretical results [10, 13]. The difference between the equilibrium energies resulting from E(v) curves of both β<sub>1</sub> and β<sub>2</sub> models ( $\Delta E = E_{\beta_1} - E_{\beta_2}$ ) was estimated about -0.05 eV/cell which is much larger than about 0.05 meV/cell [11] obtained from PP method. So, unlike PP calculations, FP-LAPW+lo calculations similar to all-electron ASW calculation [13, 38] point to β<sub>1</sub> phase as the most probable SG for the β phase hydride. The resulting bulk modulus B<sub>0</sub> through E(v) curve fitting with Murnaghan [36] are ~ 138, 133 and 132 for LaNi<sub>5</sub>, La<sub>2</sub>Ni<sub>10</sub>H<sub>14</sub> (β<sub>1</sub>) and La<sub>2</sub>Ni<sub>10</sub>H<sub>14</sub> (β<sub>2</sub>), respectively. The reduction in B<sub>0</sub> after hydrogenation is indicative of the larger compressibility of the hydride phase, with respect to parent compound, under hydrostatic pressure (Fig. 8). This is related to volume expansion of hydride compound seen earlier. It also indicates that parent compound is harder than its hydride.

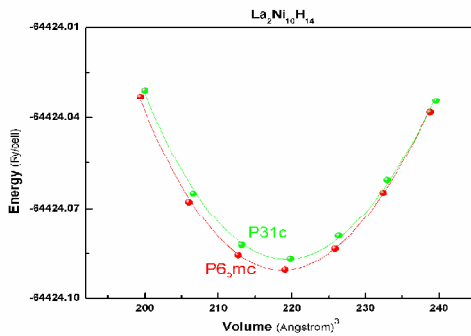


Figure 7. Volume optimization of the La<sub>2</sub>Ni<sub>10</sub>H<sub>14</sub> compound for SGs P31c and P6<sub>3</sub>mc. The solid curves are Murnaghan fits.

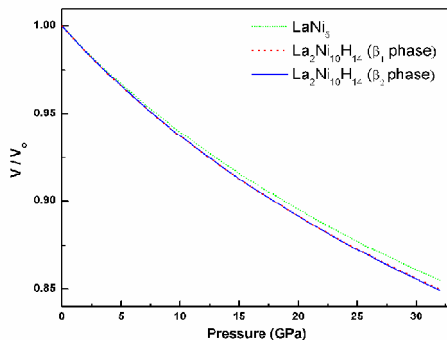


Figure 8. Variation of  $V/V_0$  with theoretical pressure,  $V_0$  is equilibrium volume.

### 3.2.2. Energetics and heat of formation

The heat of formation ( $\Delta H$ ) for an absorption reaction is one of the most important thermodynamic factors which indicates the metal hydrogen bond stability [7]. The enthalpy of formation of LaNi<sub>5</sub> and LaNi<sub>5</sub>H<sub>7</sub> (per H<sub>2</sub>) from LaNi<sub>5</sub> and H<sub>2</sub> gas are expressed by [11]:

$$\Delta H(\text{LaNi}_5) = [E(\text{LaNi}_5) - E(\text{La}) - 5E(\text{Ni})] \quad (3)$$

$$\Delta H(\text{LaNi}_5\text{H}_7) = \frac{2}{7} [E(\text{LaNi}_5\text{H}_7) - E(\text{LaNi}_5)] - E(\text{H}_2) \quad (4)$$

where  $E(\text{LaNi}_5)$ ,  $E(\text{La})$ ,  $E(\text{Ni})$  and  $E(\text{LaNi}_5\text{H}_7)$ , are the total energy of LaNi<sub>5</sub>, elemental La, elemental Ni and LaNi<sub>5</sub>H<sub>7</sub> per unit cell, respectively.  $E(\text{H}_2)$  is total energy of gaseous H<sub>2</sub> molecules evaluated with considering a big box and keeping the bond length between the two H atoms [7, 42]. In the present work, the heat of formation for LaNi<sub>5</sub> was evaluated ~ 159.3 kJ/(mol-LaNi<sub>5</sub>) which is in better agreement with experiment (159.1±8.3 kJ/mol-LaNi<sub>5</sub> [43]) compared to other theoretical work (-168 kJ/mol-LaNi<sub>5</sub> [11]). The calculated heat of formation for β<sub>1</sub> and β<sub>2</sub> phases (its hydrides) was about -39.1 and -38.4 kJ/mol-H<sub>2</sub>, respectively. These indicate that the formation of all compounds is favorable from the thermodynamic point of view, but β<sub>1</sub> phase is more stable than β<sub>2</sub>, which is in good agreement with the results. The agreement between our results and experiment (-34.8±1.8 kJ/mol-H<sub>2</sub> at 285 K for LaNi<sub>5</sub>H<sub>6.33</sub> [44]) is good in comparison with results of pseudo-potential theoretical approaches (-40 [11] and -57 [38] kJ/mol-H<sub>2</sub> at 0 K for LaNi<sub>5</sub>H<sub>7</sub>) as it was expected to be improved by using full-potential methods [38]. In the following, we employ the P6<sub>3</sub>mc structure for La<sub>2</sub>Ni<sub>10</sub>H<sub>14</sub> for our calculations.

### 3.2.3. Density of states and band structures

In this section, we study the density of states and band structures of LaNi<sub>5</sub> and LaNi<sub>5</sub>H<sub>7</sub> (P6<sub>3</sub>mc) because in the previous section we showed that SG P6<sub>3</sub>mc is more stable. Figs. 9a and b display the total (TDOS) and partial (PDOS) electronic density of states for LaNi<sub>5</sub> and its hydride, respectively. The origin of the energy scale is located at the Fermi energy ( $E_F$ ). The DOS of pure La and Ni as the constituent elements are also given for comparison. The origin of the energy scale is located at the Fermi energy ( $E_F$ ). The DOS of pure La and Ni as the constituent elements are also

given for comparison. It is clear that the TDOS of  $\text{LaNi}_5$  is composed of both bonding and non-bonding states. The band structure calculations show that the occupied states of this compound are very similar to those of constituent transition metal (pure Ni). This fact indicates that the valence band of  $\text{LaNi}_5$  is mainly derived from Ni-3d states, which is in good agreement with XPS measurements [45].

It can also be seen that the TDOS at  $E_F$  is mostly composed of Ni (2c) and Ni (3g) states. However, the contribution of Ni (3g) states is slightly increased due to the fact that Ni at 2c and 3g sites are found with the occupation ratio 2:3, respectively (considering site occupations). For parent  $\text{LaNi}_5$  compound, the narrow intensive peaks located in the range of about 0-4 eV below the Fermi energy are formed mainly by the Ni-3d states

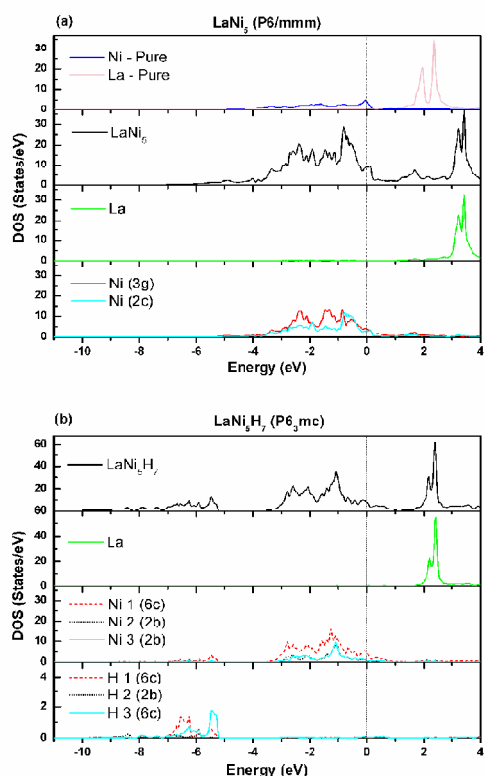


**Figure 9.** TDOS and PDOS for: (a)  $\text{LaNi}_5$  and (b)  $\text{LaNi}_5\text{H}_7$  (SG P6<sub>mc</sub>). For PDOS calculations, the site occupations were considered for Ni and H atoms.

which have dominant contribution for valence bands, while the conduction bands are generally provided by the La-4f states centered at about 3.1 eV. The DOS results are in good agreement with the other reported theoretical approaches [11, 46]. Fig. 10a shows DOS for La-5d and Ni-3d

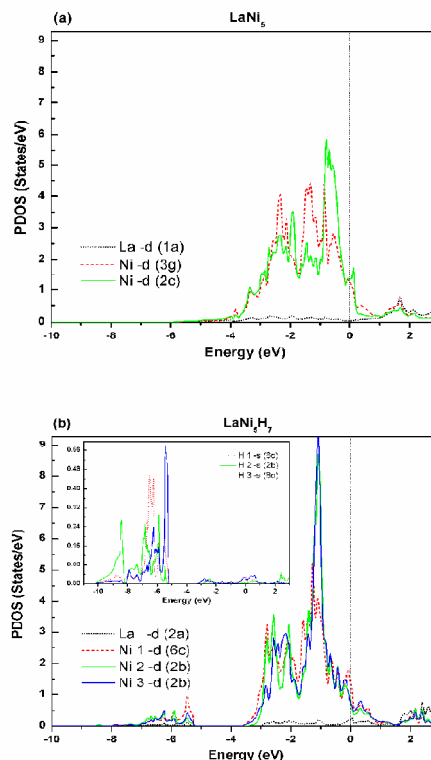


**Figure 10.** PDOS for La-d and Ni-d states in: (a)  $\text{LaNi}_5$ , and (b)  $\text{LaNi}_5\text{H}_7$ . The inset (Fig. 10b) shows PDOS for s states of H atoms.

states of  $\text{LaNi}_5$ . La states (mostly 5d) forming the bonding states are hybridized with Ni-3d band, but their contribution to the DOS at the Fermi level is very low. The bandwidth of occupied Ni-3d states is evaluated as being about 3.8 eV, which is in good agreement with ultraviolet and X-ray photoemission data [47, 48], as it is narrower than the 4.3 eV width in elemental Ni [47]. Fig. 10b shows PDOS for  $\text{LaNi}_5\text{H}_7$  compound. A comparison of TDOS for  $\text{LaNi}_5$  and its hydride shows that the sharp peak just above  $E_F$  in the  $\text{LaNi}_5$  DOS is shifted below  $E_F$  due to hydrogen absorption which can stabilize the  $\text{LaNi}_5$  saturated hydride. Moreover, a new group of states appear at energies about 5-10 eV below  $E_F$  due to hydrogenation arising from hybridization of the H 1s states with Ni, and to a lesser extent La states. These states forming 14 bands in band structure of hydride compound (Fig. 11b) are separated from those higher in energy through a gap of ~1.5 eV. However no energy gap was found for valence bands in the parent compound (Fig. 11a). From Figs 10a and b, it is also clear that the bandwidth of the occupied Ni-3d states in hydride phase (3.2 eV) is narrower than that of

its parent compound (3.9 eV), in good agreement with 3.1 eV in Ref. [11]. It can be attributed to the volume expansion of ~26% [11]. For the hydride phase, similar to the parent compound, Ni-3d states have dominant contribution at  $E_F$  and among these states, Ni1 have the most intensity with respect to all the other atomic constituents which is related to the presence of Ni1 in all three hydrogen insertion sites. So, it is expected that the Ni1-H interaction be dominant. the Ni1-H interaction be dominant.

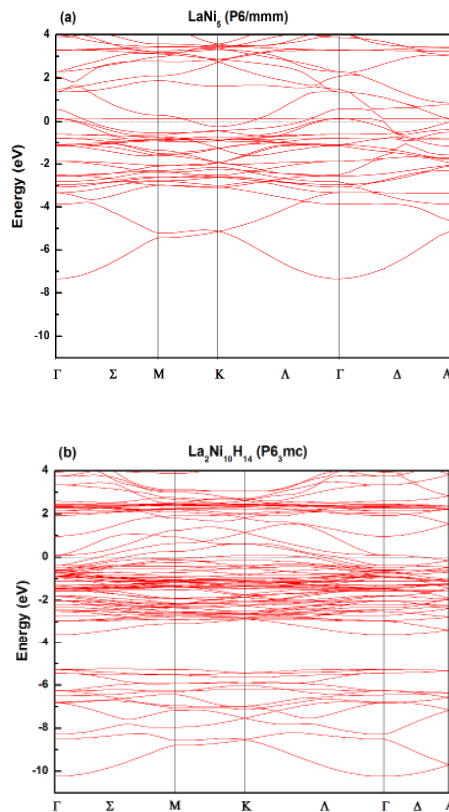


**Figure 11.** Energy band structures of (a)  $\text{LaNi}_5$  and (b)  $\text{La}_2\text{Ni}_{10}\text{H}_{14}$  ( $P6_3mc$ ).

We also obtained the intensity of DOS at Fermi level,  $n(E_F)$ , for  $\text{LaNi}_5$  and  $\text{LaNi}_5\text{H}_7$ , of about 8.98 and 7.54 states/eV-f.u., respectively. Decrease in DOS at  $E_F$  for hydride phase can be due to the filling of Ni-3d band as a result of hydrogen absorption. The electronic-specific heat coefficient [11], expressed by  $\gamma = \frac{\pi^2}{3} k^2 n(E_F)$ , was calculated. The  $\gamma = 21.18$  and  $17.77$  mJ/mol-K<sup>2</sup> obtained for  $\text{LaNi}_5$  and its hydride are in good agreement with the experimental heat capacity measurements and with 21.7 and 17.44 mJ/mol-K<sup>2</sup> of Hector et al. [11].

#### 4. Conclusion

In this paper, the structural, morphological and hydrogenation properties of the  $\text{LaNi}_5$  hydrogen storage alloy have been investigated. XRD analyses revealed that after 30 H/D cycling, the depletion of Ni fine particles occurred on the surface of  $\text{LaNi}_5$ , as some weak peaks corresponding to pure nickel phase also appeared. In addition, the crystallite size of alloy decreases after H/D cycling while the lattice strain increases. After H/D cycling, the particle size decreases and also its distribution becomes nearly uniform compared to non-cycled alloy. The hydriding kinetic measurements showed that the Cwt. % increases with the applied pressure at constant temperature, while it decreases with temperature under constant applied pressure conditions. However, the hydriding reaction rates increase with temperature. The theoretical part of this study is related to the structural, energetic and electronic properties of  $\text{LaNi}_5$  and its saturated hydride using FP-LAPW+lo method. The results indicated a unit cell volume expansion of ~26% for hydride sample due to hydrogen insertion in interstitial sites. However, after hydrogenation, the bulk modulus decreases. The formation of all compounds was favorable from the thermodynamical point of view. The band structure calculations of  $\text{LaNi}_5$  showed that the valence band is mainly derived from Ni-3d states, and is in good agreement with XPS measurements. It was also seen that the bandwidth of the occupied Ni-3d states in hydride phase was narrower than that of the parent compound, because of volume expansion. However, intensity of DOS at  $E_F$  and hence the electronic-specific heat coefficient decreases after hydrogenation which can be due to the filling of Ni-3d band as a result of hydrogen absorption.

#### Acknowledgments

The authors would like to thank the Renewable Energies Organization of Iran (SUNA) for their financial support.

## 5. References

- [1] Hirscher M., Handbook of Hydrogen Storage: New Materials for Future Energy Storage, Wiley-VCH. Press, 2010.
- [2] Broom D. P., Hydrogen Storage Materials, Green Energy and Technology, Springer-Verlag, 2011.
- [3] Alefeld G. and Völkl J., Hydrogen in Metals II, Topics in Applied Physics, Springer-Verlag, 1978.
- [4] Zhu K. G., Shi J. Z. and Zhang L.D., "Effect of temperature on electrical resistivity of a hydrogenated LaNi<sub>5</sub> thin film", Chin. Phys., 1998, 7: 504
- [5] Lin S. J. and Zheng H. P., "Electronic structure of the surface of LaNi<sub>5</sub> crystal", Acta Phys. Sin., 2005, 10: 4680
- [6] Rozdzynska-Kielbik B., Iwasieczko W., Druelis H., Pavlyuk V.V. and Bala, H., "Hydrogenation equilibria characteristics of LaNi<sub>5</sub>-xZnx intermetallics", J. Alloys Comp., 2000, 298: 237
- [7] Zareii S. M. and Sarhaddi R., "Structural, electronic properties and heat of formation of Mg<sub>2</sub>FeH<sub>6</sub> complex hydride: an ab initio study", Phys. Scr., 2012, 86: 015701
- [8] Mungole M. N., Balasubramaniam R. and Rai K. N., "Magnetization behavior of hydrogen storage MmNi<sub>5</sub> intermetallics with Al, Mn and Sn substitutions", Int. J. Hydrogen Energy, 1997, 22: 679
- [9] Biris A., Bucur R.V., Ghete P., Indrea E. and Lupu D., "The solubility of deuterium in LaNi<sub>5</sub>", J. Less-Common Met., 1976, 49: 477
- [10] Tatsumi K., Tanaka I., Inui H., Tanaka K., Yamaguchi M. and Adachi H., "Atomic structures and energetics of LaNi<sub>5</sub>-H solid solution and hydrides", Phys. Rev. B, 2001, 64: 184105.
- [11] Hector Jr L.G., Herbst J. F. and Capehart T. W., "Electronic structure calculations for LaNi<sub>5</sub> and LaNi<sub>5</sub>H<sub>7</sub>: energetics and elastic properties", J. Alloys Comp., 2003, 353: 74.
- [12] Lartigue C., Le Bail A. and Percheron-Guegan A., "A new study of the structure of LaNi<sub>5</sub>D<sub>6.7</sub> using a modified Rietveld method for the refinement of neutron powder diffraction data", J. Less-Common Met., 1987, 129: 65
- [13] Al Alam A. F., Matar S. F., Nakhl M. and Ouaini N., "Investigation of changes in crystal and electronic structures by hydrogen within LaNi<sub>5</sub> from first-principles", Solid State Sciences, 2009, 11: 1098
- [14] Blaha P., Schwarz K., Madsen G. K. H., Kvanicka D. and Luitz J., An Augmented Plane Wave Plus Local Orbitals Program for Calculating Crystal Properties, Vienna University of Technology, 2001.
- [15] www.wien2k.at
- [16] Perdew J. P., Burke K. and Ernzerhof M., "Generalized Gradient Approximation Made Simple", Phys. Rev. Lett., 1996, 77: 3865
- [17] Blochl P. E., Jepsen O. and Andersen O. K., "Improved tetrahedron method for Brillouin-zone integrations", Phys. Rev. B, 2004, 49: 16223
- [18] Nakamura Y., Sato K., Fujitani S., Nishio K., Oguro K. and Uehara I., "Lattice expanding behavior and degradation of LaNi<sub>5</sub>-based alloys", J. Alloys Comp., 1998, 267: 205
- [19] Srivastava S. and Upadhyaya R. K., "Investigations of AB<sub>5</sub>-type hydrogen storage materials with enhanced hydrogen storage capacity", Int. J. Hydrogen Energy, 2001, 36: 7114
- [20] Ahn H. J. and Lee J. Y., "Intrinsic degradation of LaNi<sub>5</sub> by the temperature induced hydrogen absorption-desorption cycling", Int. J. Hydrogen Energy, 1991, 16: 93
- [21] Tian X., Liu X-d., Xu J., Feng H-w., Chi B., Huang L-H and Yan S-F., "Microstructures and electrochemical characteristics of Mm<sub>0.3</sub>M<sub>10.7</sub>Ni<sub>3.55</sub>Co<sub>0.75</sub>Mn<sub>0.4</sub>Al<sub>0.3</sub> hydrogen storage alloys prepared by mechanical alloying", Int. J. Hydrogen Energy, 2009, 34: 2295
- [22] Cerny R., Joubert J.-M., Latroche M., Percheron-Guegan A. and Yvon K., "Anisotropic diffraction peak broadening and dislocation substructure in hydrogen-cycled LaNi<sub>5</sub> and substitutional derivatives", J. Appl. Cryst., 2000, 33: 997

- [23] Srivastava S. and Srivastava O. N., "Investigations of synthesis and characterization of  $\text{MmNi}_{4.3}\text{Al}_{0.3}\text{Mn}_{0.4}$  and  $\text{MmNi}_{4.0}\text{Al}_{0.3}\text{Mn}_{0.4}\text{Si}_{0.3}$  hydrogen storage materials through thermal and spin melting processes", *Int. J. Hydrogen Energy*, 1998, 23: 7
- [24] Li S.L., Chen W., Chen D.M. and Yang K., "Effect of long-term hydrogen absorption/desorption cycling on hydrogen storage properties of  $\text{MmNi}_{3.55}\text{Co}_{0.75}\text{Mn}_{0.4}\text{Al}_{0.3}$ ", *J. Alloys Compd.*, 2009, 474:164
- [25] Li S.L., Chen W., Luo G., Han X.B., Chen D.M., Yang K. and Chen W.P., "Effect of hydrogen absorption/desorption cycling on hydrogen storage properties of a  $\text{LaNi}_{3.8}\text{Al}_{1.0}\text{Mn}_{0.2}$  alloy", *Int. J. Hydrogen Energy*, 2012, 37:3268
- [26] Johnson D. G. and Pangborn J. B., *ibid.*, 1980, 73: 127
- [27] Zhang T. B., Wang X. F., Hu R., Li J. S., Yang X. W., Xue X. Y. and Fu H. Z., "Hydrogen absorption properties of  $\text{Zr}(\text{V}_{1-x}\text{Fe}_x)_2$  intermetallic compounds", *Int. J. Hydrogen Energy*, 2012, 37: 2328
- [28] Ivey D. G. and Northwood D. O., "Storing energy in metal hydrides: a review of the physical metallurgy", *J. Mater. Sci.*, 1983, 18: 321
- [29] Haberman Z., Bloch J., Mintz M. H. and I Jacob I., "Kinetics of hydride formation in massive  $\text{LaAl}_{0.25}\text{Ni}_{4.75}$  samples", *J. Alloys Compd.*, 1997, 253-254: 556.
- [30] Muthukumar P., Satheesh A., Linde M., Mertz R. and Groll M., "Studies on hydriding kinetics of some La-based metal hydride alloys", *Int. J. Hydrogen Energy*, 2009, 34: 7253.
- [31] Ming L., Lavendar E., Goudy A.J., "The hydriding and dehydriding kinetics of some  $\text{RCo}_5$  alloys", *Int. J. Hydrogen Energy*, 1997, 22: 63.
- [32] Chou K. C., Xu K. D., "A new model for hydriding and dehydriding reactions in intermetallics", *Intermetallics*, 2007, 15: 767.
- [33] Zhang X., Li Q. and Chou K. C., "Kinetics of hydrogen absorption in the solid solution region for Laves phase  $\text{Ho}_{1-x}\text{Mm}_x\text{Co}_2$  ( $x = 0, 0.2$  and  $0.4$ ) alloys", *Intermetallics*, 2008, 16:1258.
- [34] Jander W., Reaktionen im festen Zustande bei höheren Temperaturen. Reaktionsgeschwindigkeiten endotherm verlaufender Umsetzungen, *Z. Anorg. Allg. Chem.*, 1927, 163: 1.
- [35] Johnson W. A. and Mehl R. F., "Reaction kinetics in processes of nucleation and growth", *Trans. Am. Inst. Min. Metall. Eng.*, 1939, 135: 416.
- [36] Murnaghan F. D., "The Compressibility of Media under Extreme Pressures"; *Proc. Natl. Acad. Sci. USA*, 1944, 30: 244.
- [37] Feynman R. P., "Forces in Molecules", *Phys. Rev.*, 1939, 56: 340.
- [38] Nakamura H., Nguyen-Manh D. and Pettifor D.G., "Electronic structure and energetics of  $\text{LaNi}_5$ ,  $\alpha\text{-La}_2\text{Ni}_{10}\text{H}$  and  $\beta\text{-La}_2\text{Ni}_{10}\text{H}_{14}$ ", *J. Alloys Compd.*, 1998, 281: 81
- [39] Berezniatsky M., Ode A., Hightower J. E., Yeheskel O., Jacob I. and Leisure R. G., "Elastic moduli of polycrystalline  $\text{LaAl}_x\text{Ni}_{5-x}$ ", *J. Appl. Phys.*, 2002, 91: 5010.
- [40] Brouha M. and Buschow K. H. J., "Magnetic properties of  $\text{LaCo}_{5x}\text{Ni}_{5-5x}$ ", *J. Phys. F: Metal Phys.*, 1975, 5: 543.
- [41] Tanaka K., Okazaki S., Ichitsubo T., Yamamoto T., Inui H., Yamguchi M. and Koiwa M., "Evaluation of elastic strain energy associated with the formation of hydride precipitates in  $\text{LaNi}_5$ ", *Intermetallics*, 2000, 8: 613.
- [42] Bouhadda Y., Rabehi A., Boudouma Y., Feni-neche N., Drablia S. and Meradji H., "Hydrogen solid storage: First-principles study of  $\text{ZrNiH}_3$ ", *Int. J. Hydrogen Energy*, 2009, 34: 4997.
- [43] Hubbard W. N., Rawlins P. L., Connick P. A., Stedwell Jr R. E. and O'Hare P. A. G., "The standard enthalpy of formation of  $\text{LaNi}_5$ . The enthalpies of hydriding of  $\text{LaNi}_{5-x}\text{Al}_x$ ", *The Journal of Chemical Thermodynamics*, 1983, 15: 785.
- [44] Murray J. J., Post M. L. and Taylor J. B., "The thermodynamics of the  $\text{LaNi}_5\text{-H}_2$  system by differential heat flow calorimetry II: The  $\alpha$  and  $\beta$  single-phase regions", *J. Less-Common Met.*, 1981, 80: 211.

[45] Wallace W.E. and Pourarian. F., "Photoemission Studies of  $\text{LaNi}_{5-x}\text{Cu}_x$  Alloys and Relation to Hydride Formation", *J. Phys. Chem.*, 1982, 86: 4958.

[46] Knyazev Y. V., Lukoyanov A. V., Kuzmin Y. I. and Kuchin A. G., "Effect of Cu-doping on the electronic structure and optical properties of  $\text{LaNi}_5$ ", *J. Alloys Comp.*, 2011, 509: 5238.

[47] Fuggle J. C., Hillebrecht F. U., Zeller R., Zolnierok Z., Bennett P. A. and Freiburg Ch., "Electronic structure of Ni and Pd alloys. I. X-ray photoelectron spectroscopy of the valence bands", *Phys. Rev. B*, 1982, 27: 2145.

[48] Weaver J. H., Franciosi A., Wallace W. E. and Smith H. K., "Electronic structure and surface oxidation of  $\text{LaNi}_5$ ,  $\text{Er}_6\text{Mn}_{23}$ , and related systems", *J. Appl. Phys.*, 1980, 51: 5847.